How competitive species such as buffer solutions influence the adsorption of dyes onto photocatalyst TiO2 particles

Title: How competitive species such as buffer solutions influence the adsorption of dyes onto photocatalyst TiO_2 particles

Authors: Ganna Darmograi, Monika Kus, Gaelle Martin-gassin, Jerzy Zajac, Sara Cavaliere, Benedicte Prelot

PII: S0025-5408(16)32647-2
DOI: http://dx.doi.org/doi:10.1016/j.materresbull.2017.05.025
Reference: MRB 9340

To appear in: *MRB*

Received date: 16-12-2016
Revised date: 9-5-2017
Accepted date: 9-5-2017

Please cite this article as: Ganna Darmograi, Monika Kus, Gaelle Martin-gassin, Jerzy Zajac, Sara Cavaliere, Benedicte Prelot, How competitive species such as buffer solutions influence the adsorption of dyes onto photocatalyst TiO2 particles, Materials Research Bulletinhttp://dx.doi.org/10.1016/j.materresbull.2017.05.025

How competitive species such as buffer solutions influence the adsorption of dyes onto photocatalyst TiO_2 particles

Ganna DARMOGRAI [1], Monika KUS [2], Gaelle MARTIN-GASSIN [1], Jerzy ZAJAC [1],

*Sara CAVALIERE *[1], Benedicte PRELOT *[1]*

1 Institut Charles Gerhardt, UMR-5253 CNRS-UM-ENSCM, C.C. 1502, Place Eugène Bataillon, F-34095 Montpellier cedex 5, FRANCE

2 Laboratory of Adsorption and Catalysis, Department of Chemistry, University of Antwerpen, Campus Drie Eiken, Universiteitsplein 1, B-2610 Wilrijk, BELGIUM

* Correspondence: benedicte.prelot@umontpellier.fr ; Tel.: +33 4 67 14 33 05

sara.cavaliere@umontpellier.fr ; Tel.: +33 4 67 14 90 98

Graphical abstract

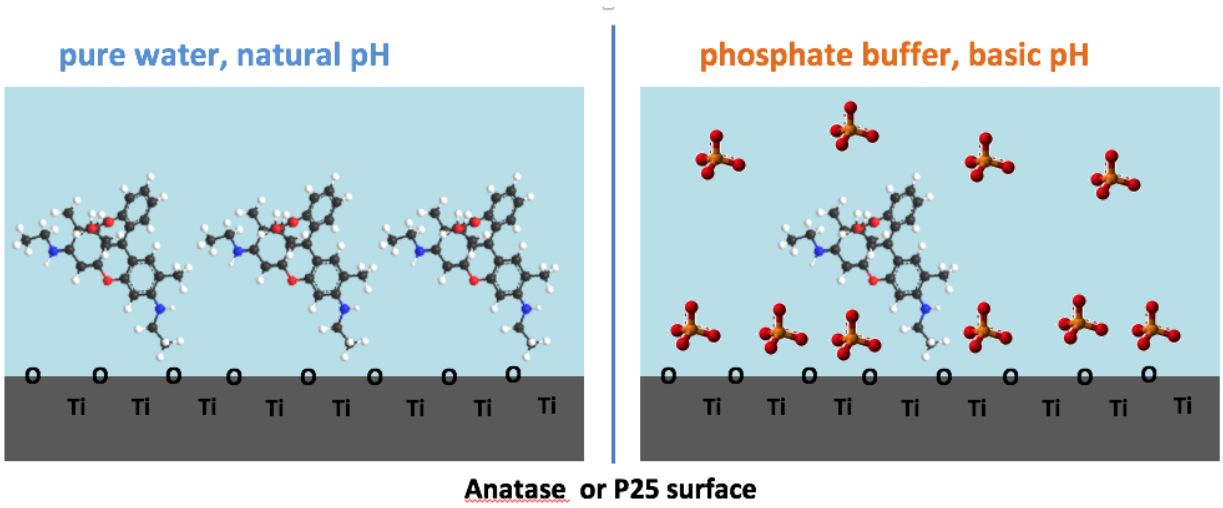

Highlights

- Rhodamine 6G adsorption in water at natural pH and in phosphate buffer pH 6 and 8.
- Influence of nano-structure of Ti-based materials on Rhodamine 6G retention.
- Data expressed in µmol g^{-1} and µmol m^{-2} are discussed.
- Competition between the dye molecules and phosphates on the TiO_2 surface.
- Various sorption affinity of rutile and anatase for phosphate species.

ABSTRACT:

Various titanium based materials were chosen to obtain series of solids with various properties (structure, texture, morphology, surface reactivity…): nanopowder P25 and commercial Anatase; ElectroSpun nanofibres; trititanate nanotubes and mixed-phase anatase/trititanate. The adsorption of Rhodamine 6G was studied at natural pH and from phosphate buffer 0.1M at different pHs. The adsorption capacities were dependent of the type of particles and the nature and pH of the

solutions. Anatase and ES nanofibres had the lowest and the highest adsorption capacity respectively, with lower sorption at pH 6 due to the negative surface charge. This effect was rather small in the case of Anatase, which exhibits huge phosphate species adsorption. This demonstrates the competition between anionic species, and its consequence on the affinity for Rhodamine 6G in the presence of PO_4^{3-}.

KEYWORDS:

photocatalyst, titanium oxides, titanate, Rhodamine 6G, adsorption, competition, phosphate buffer.

1. Introduction

In recent years, titanium dioxide has attracted much attention in environmental applications for example the treatment of dye-containing wastewater. Because of their powerful oxidation strength, high chemical and photo-stability in water, nontoxicity, low cost, and insolubility in water under most environmental conditions, they have shown great potential as ideal and powerful photocatalysts [1-3]. The optimization of catalysts performance is based on the understanding of the main driving forces and mechanisms for their oxidative removal [4], and especially the selectivity of adsorbent that can be affected by many factors such as properties of the reactant (size, polarity, structure, etc.), surface charging, solvent, surface atomic structure. Numerous studies have been carried out to better explain TiO_2 surface chemistry and especially at the solid-liquid interface [5]. Because most organic pollutants have weak adsorption on the TiO_2 particles, surface treatment or textural modification could enhance the adsorption capacity and potentially their photocatalytic properties when they are used in degradation process [6-9]. In various shapes/morphologies, such as nanoparticles, tubes, wires, fibres etc…, nanomaterials

show a better performance in environmental remediation than other conventional techniques because of their high surface-to-volume ratio [10] especially when using innovative synthesis for original one-dimensional (1D) electrospun nanostructured materials [11-15] or tubes such as titanate nanotubes [16, 17].

The morphology, the textural properties, the crystallinity play crucial roles on surface reactivity [18-21]. Indeed, various acidic character and location of polar sites on the TiO_2 surface [22, 23] or differences in proton affinity distributions (PADs) and the strength (pK position) of various local domains of proton adsorption [24] have been observed on anatase with various shapes and exposed surfaces. Local charge, local arrangements or distortions, fine mixture of phase, may affect the sorption capacity. The complexity of the liquid-solid interface implies to consider more variables in comparison to the gas-solid system, with parameters such as the surface site, preparation procedures, and concentration of the particles, the pH of the solution and its effect on the surface structure, the concentration of the reactants, … [1]. These include also the control of the surface charge by adjusting the pH [25, 26], anchoring specific molecules to the surface for the selective adsorption of reactants [7, 27] and even some times the idea of the competitive solute solvent adsorption [28].

Competitive adsorption onto TiO_2 surfaces is studied in different manners. Yang and Davis [29] reported Cu(II) and EDTA adsorption from single and bi-component systems onto P25 TiO_2 sample. They have shown that the behaviour in single component system was strongly modified when ionic and cationic species were mixed, with the occurrence of ligand bridged ternary complexes. In the case of glutamate and lysine molecules in the presence of Ca^{2+}, Lee et al. [30] have evidenced cooperative, or competitive, effects, depending on the modification of surface charge after adsorption of Ca^{2+}, inducing attraction or repulsion of the organic species to be the adsorbed. Weng et al [31] have shown that in the presence of humic (HA) or fulvic (FA) acids

together with phosphate, the sorption on goethite FeOOH exhibits much stronger competition effects of FA in comparison with HA, in relation with the difference in the spatial distribution more or less close to the oxide surface. In some cases, when the sorption is performed in buffers [32], the sorption of humic acids (HA) in phosphate buffer may be reduced, not only due to the effect of pH or ionic strength, but phosphate might compete with HA on the surface of adsorbent, or may interact with the HA in the solution and affecting HA adsorption.

To evidence the influence of competitive effect in particular in presence of phosphate, adsorption of Rhodamine 6G, a cationic orange-fluorescent dye often used in degradation tests was extensively studied in different conditions (in water or in buffer, at various pHs), in order to establish the influence of physicochemical conditions. Different types of Titanium based nanomaterials, nanopowder (P25, Anatase Commercial), nanofibres and nanotubes in two forms calcined and not calcined, denoted TNT-C and TNT-NC, respectively, were chosen as adsorbent for the organic dye Rhodamine 6G. Nanotubes and ES nanofibres samples were prepared using a hydrothermal chemical route and electrospinning method, respectively. As reference, commercial P25 and Anatase commercial Nanopowder were used. In the end, the sorption properties were correlated with the competitive character of the mechanism on the surface active sites.

2. Experimental section

2.1. Materials and syntheses of adsorbents / photocatalysts

The dye Rhodamine 6G was purchased from E. Merck India. The formula is shown on the Figure 1 and was labelled Rh6G. Commercial TiO_2 nanopowder P25 was obtained from Degussa AG and Titanium (IV) oxide, Anatase from Aldrich. They were used as received. The phosphate buffers and all solutions of Rh6G were prepared in ultrapure water (resistivity of 18.2 MΩ)

produced by using an Elga LabWater Model PL 5241 system. Nanofibres and nanotubes were prepared using the conditions described in the following.

2.1.1. Electrospun ES nanofibres

For the synthesis of TiO_2 ES nanofibres, a procedure similar to that in [33] was followed. A carrier polymer solution made of 230 mg of polyvinyl pyrrolidone (PVP, M_w ~1,300,000, Aldrich) in 3.3 mL of absolute ethanol (puriss., Sigma-Aldrich) was added to a precursor solution made of 0.52 mL of titanium(IV) isopropoxide (97 %, Aldrich, stored in a glove box) and 1 mL of acetic acid (Sigma-Aldrich). The solutions were degassed by ultrasonication for 15 min, mixed together, stirred for 1 hour and loaded into the syringe. Electrospinning of the final solution was carried out in air at room temperature with a standard syringe and a grounded collector plate configuration with the following conditions: distance between the needle tip and the collector plate of 10 cm, applied voltage of 15 kV and flow rate of 0.5 mL h^{-1}. The as-prepared fibres were calcined in air at 500 °C at a heating rate of 5 °C min^{-1} for 6 hours in order to decompose and remove PVP and obtain pure inorganic fibres.

2.1.2. Nanotubes

For preparation of tubes 4.5 g of TiO_2 (Sigma Aldrich) was dispersed into 80 ml of 10 M NaOH (Acros Organics) and stirred for 1 hour. Further, the mixture was transferred to an autoclave and kept in an oven at 150˚C for 48 hours. The obtained solid was recovered by centrifugation and further washed with distilled water, which resulted in sodium trititanate nanotubes. Afterwards, the sample was ion-exchanged by stirring the obtained material for 30 min in 480 ml of 0.1 M solution of HCl at room temperature. The sample was recovered by centrifugation and further washed three times with water and two times with ethanol. Finally, the washed sample was dried at 100˚C for 3 days. The as-obtained samples are denoted as TNT NC.

Some of the material was calcined in order to change the content of anatase in the sample (re-crystallization while maintaining morphology) according to the following procedure 1 °C min^{-1} to 350°C for duration of 6 hours in ambient atmosphere followed by stepwise cooling. The obtained calcined material is denoted as TNT C.

3.2. Characterization of the solid materials

The specific surface areas S_{BET} (m^2 g^{-1}) were deduced from nitrogen adsorption at -196°C using a Micromeritics ASAP2020 and calculated with the Brunauer-Emmet-Teller BET method. The samples were previously outgassed at 200°C for 16 h under a residual pressure of 10^{-2} Pa. The crystal phase of the titanium nanoparticles was determined by X-ray diffraction (XRD) on a PANAlytical X'pert powder diffractometer equipped with CuK_α radiation (λ = 1.542 Å) and by FT-Raman spectroscopy [34, 35]. The morphology of all samples was analysed by using a Hitachi S-4800 scanning electron microscope (SEM).

3.3. Isotherms of Rhodamine 6G adsorption

Adsorption of Rh6G was carried out using a batch process, in pure water or in buffer. Phosphate buffer solutions (0.1 mol L^{-1}) were used throughout the experiment to maintain a pH value of 6.0 or 8.0. They were prepared by mixing various amounts of two stock solutions, 0.2 mol L^{-1} monobasic and 0.2 mol L^{-1} dibasic sodium phosphate. For pH 6, the volumes are 87.7 ml and 12.3 ml of $NaH_2PO_4 \cdot H_2O$ and Na_2HPO_4 respectively, with ultrapure water to 200 ml. For pH 8, the volumes are 5.3 ml and 94.7 ml with ultrapure water to 200 ml. The same buffer solution was used to prepare Rh6G stock solution with concentration 10 µmol L^{-1}. It was then diluted to prepare the solutions at various initial concentrations (0.25 - 10 µmol L^{-1}) for the various experimental points on the adsorption isotherm. In each tube, a solid sample of titanium oxide (5 mg) was dispersed in 10 ml Rh6G solution of already known initial concentration. Then, the

tubes were stirred overnight at 25°C by using a rotary shaker at 10 rpm to obtain adsorption equilibrium. The pH of the suspension was then carefully checked. The separation of the solid phase from the liquid was achieved by centrifugation at 10 000 rpm for 12 min. The supernatant was then analysed by using V-670 UV-Vis Spectrophotometer (interval of wavelength 400-600 nm) to determine the equilibrium concentration. The adsorption capacity (Q_{ads}, μmol m^{-2}) is the calculated as follows and displayed as function of equilibrium concentration.

$$Q_{ads} = \frac{V_o(C_i - C_{eq})}{m_S S_{BET}}$$

C_i and C_{eq} are the initial and final (equilibrium) concentration of Rh6G respectively expressed in μmol L^{-1}, V_o (L) is the initial volume of the sample solution, and m_s and S_{BET} are the weight (in g) and the specific surface area (in m^2 g^{-1}) of the adsorbent, respectively.

3.4. Zeta Potential measurements

The dependence of ζ potential on pH was studied in aqueous suspension with a concentration of 1 mg L^{-1} for all investigated samples, by using the Malvern instrument Zetasizer 3000HSa. The pH values of the aqueous mixtures were adjusted, adding 1 mol L^{-1} HCl and 1 mol L^{-1} NaOH, respectively. Zeta potentials for different solids were measured in phosphate buffer solutions at pH 8.

3. Results

The Figure 2 shows the Scanning Electron Microscopy (SEM) images of the variousTiO_2 samples. The P25 nanopowder is known to exhibit spherical primary particles with 21 nm, with significant aggregation of the elementary particles. The Anatase is also composed of agglomerated nanoparticles (10-20 nm). The ES nanofibres are very long filaments, with 100-

200 nm diameters and several μm in length. TNT (NC or C) display needles or flakes with 10 nm thickness and 1 μm length.

Table 1 summarizes the characteristic of all commercial and synthesized materials used in this work. Concerning the textural parameters, two classes of materials could be distinguished, each of them has the similar specific surface area. The first set of materials, with nanotubes TNT, exhibit high S_{BET}, 342 and 340 $m^2 g^{-1}$ for not calcined and calcined samples respectively. Their specific surface areas are approximately seven times higher than that of the three other samples, which possess S_{BET} between 46 and 57 $m^2 g^{-1}$. On the other hand, XRD analysis (data shown in ESI) confirmed that the commercial anatase sample is pure anatase phase. Besides, P25 and ES nanofibres contain the mixture of rutile and anatase phases, with mainly anatase in both cases [36]. For nanotubes, the not calcined sample contain only TNT phase, whereas a small percentage of anatase appears after calcination as detected by FT-Raman Spectroscopy [35].

In order to evaluate the influence of both surface charge and pH, the dye adsorption was performed at natural pH (pH 5.2-5.7) and in phosphate buffer at two different pHs, pH 6 and pH 8. The adsorption isotherms of Rh6G on the spherical nanoparticles P25 are presented on Figure 3. Maximum amounts of dye adsorbed on all titanium oxide samples from H_2O at natural pH and from phosphate buffer solution at pH 8 and pH 6 are compared for all samples on Figure 4. The maximum is evaluated for high equilibrium concentration, when the amount adsorbed seems to reach a pseudo plateau. In buffered solutions, it can be noticed that for P25 adsorption capacity increases from 0.8×10^{-2} μmol m^{-2} to 1.5×10^{-2} μmol m^{-2} with increasing pH from 6 to 8 respectively. These amounts are very low, especially when compared with the ones obtained on modified solid, for example in the case of Tada's work [7], in which experimental conditions or

surface treatment could increase 2.6-fold the saturated adsorption amount. It is well known that the adsorption onto oxides with variable surface charge is strongly pH dependent. The PZC of the materials are slightly different. Even if the sorption is performed at similar pH, the surface charge if the materials may be different. Since the point of zero charge (PZC) of P25 is evaluated at pH ≈ 6 [37], adsorption of cationic molecule Rh6G is favoured under basic conditions compared to acidic conditions in similar ionic strength or without competing species and specific interactions [38]. When pH increases from 6 to 8, Rh6G is more easily attracted by the P25 surface, and the adsorption is more favourable as observed on Figure 3. This result points to importance of electrostatic interaction between Rh6G and the surface of the adsorbent.

For commercial Anatase nanoparticles (Figure 1 in ESI), the difference between the maximum adsorbed at pH=6 and pH=8 is not significant (0.48×10^{-2} and 0.51×10^{-2} μmol m^{-2} respectively, within the experimental error range). It can be explained by the limited affinity of the Anatase sample for the dye adsorption from the buffer solutions. In contrast to the P25 for which the adsorption is pH dependent, the increase of pH has no influence on the amount adsorbed onto Anatase. In both cases for P25 and Anatase on Figure 4, the adsorption capacity in pure water, at natural pH (5.2-5.7 for P25, 4.7-5.3 for Anatase), is 4 or 5 times higher than in buffer solution. This cannot be explained by the simple influence of pH, since adsorption should be lower at acid pH when the surface charge decreases. One of the aim of this study was also to evaluate the modification of sorption capacity when photocatalysts are nanostructured, and display specific morphology, sometimes together with high specific surface areas. Sorption properties were evaluated for fibres of anatase-rutile mixture and for calcined and not calcined trititanate nanotubes. The obtained results are shown on Figure and Figure 6. The comparisons of the maximum adsorption capacity in different media are shown on Figure 4. Similar conclusions are

drawn for nanotubes and ES nanofibres. Adsorbed quantities for not calcined and calcined tubes are lower in the buffer solution (0.9 x 10^{-2} µmol m^{-2} and 1 x 10^{-2} µmol m^{-2}, respectively), than those in water (4.8 x 10^{-2} µmol m^{-2} and 2.7 x 10^{-2} µmol m^{-2}). This effect is less obvious in the case of electrospun fibres for which only the sorption in buffer at pH 6 of lower. Indeed, for ES nanofibres maximum adsorbed amount from buffer at pH=6 is 4.7 x 10^{-2} µmol m^{-2} while it increases in the range 8 to 10 x 10^{-2} µmol m^{-2} at pH=8, whereas it reaches 12 or 14 in water 10^{-2} µmol m^{-2}.

The Figure 4 confirms that the specific shape of this solids and their morphology increase the adsorption capacity. Furthermore, the comparison of TNT-NC and TNT-C shows the contribution of anatase in calcined sample. The adsorption onto anatase is lower compared to pure TNT, and the total adsorption is lower on calcined nanotubes, compared to raw material before calcination. But it is important to mention that the tendency of the maximum adsorption between samples is strongly dependant on how it is evaluated. In µmol/g (Figure 4 B), the tube exhibit the higher capacity. But when normalized using the specific surface area (µmol/m^2 Figure 4 A), the electrospun fibres are performing.

For all samples, there is an increase of the amount adsorbed in the pure water (see Figure 4), in comparison with experiments in the buffer solution. In order to clarify these differences in adsorption, zeta-potential measurements were carried out. Figure S2 in ESI shows the results obtained for all titanium oxide particles at pH 8 in water (pH adjusted with NaOH) and pH 8 in buffer solution. Except for calcined nanotubes in water, the values of zeta potential are negative

for all samples. This result was expected since IEP of rutile and anatase are evaluated at pH 5.8-6, whereas it is evaluated at 3 or 4 for TNT depending on their synthesis conditions [16]. As it can be observed, zeta potential values measured in buffer are higher than the values obtained in water (except for not calcined nanotubes). It shows clearly the influence of the buffer on the surface properties of adsorbents. Theoretically, because of the higher zeta potential of the surfaces in buffer solution, Rh6G should be more attracted and more adsorbed in buffer surroundings. Nevertheless, Rh6G is more adsorbed in water, with lower values of zeta potential.

In order to explain the difference between Rh6G adsorption on Anatase and P25 from the buffer solutions at different pHs, adsorption of phosphates on these two solids was performed. Results of the adsorption isotherms of HPO_4^{2-} are shown on Figure 7. It can be observed that Anatase exhibited completely different behaviour compared to P25. Phosphate adsorption onto P25 is insignificant (1.5 10^{-2} µmol m^{-2}), whereas Anatase displays high adsorption capacity (Q max = 0.9 µmol m^{-2} i.e. 90 10^{-2} µmol m^{-2}), and higher affinity toward phosphate species. From these data, it is obvious that for Anatase particle, phosphates are highly adsorbed. This firstly explains the decrease of adsorption capacity in buffer solution compared to measurements in pure water. Moreover, this is the evidence of the presence of the competitive adsorption between the Rh6G molecules and the phosphates on the titanium oxide surfaces. Similar competition behaviour was already reported for humic or fulvic acids onto titanium dioxide nanoparticles from phosphate buffer solutions [32] or goethite in the presence of phosphate [31].

When adsorption of the dye is performed in buffer solution, the competitive adsorption between phosphate and dye takes place. Surface sites are strongly hindered by phosphate species, which are adsorbed on it. They are thus not available for dye adsorption. Finally, the influence of

pH is negligible, since, even if the surface charge is higher at pH 8, all the new ionized sites are occupied by phosphate. Anatase is more affected by adsorption of phosphates, and that is why there is no difference in adsorption capacity at pH 6 or 8 for this sample. In the case of P25, the sites are less sensitive to phosphate sorption. However, in the buffer solution, there is still slight effect of pH, with 0.8 and 1.6 10^{-2} µmol m^{-2} for pH 6 and pH 8 respectively. The strength of the interaction between TiO_2 and phosphate species was also evidenced by Connor et McQuillan. From phosphate absorbance collected with internal reflection spectroscopy they obtained isotherm typical of a strongly binding adsorbate, with adsorption increasing to saturation coverage at relatively low concentrations. They observed that phosphate binds strongly to TiO_2 surface through surface complexes and influences the interfacial and surface chemistry of TiO_2 [39].

Furthermore, for the TNT, maximum adsorbed amounts were influenced by calcination treatment, with higher adsorption for NC samples 4.8 x 10^{-2} µmol m^{-2} compared to calcined solids (2.7 x 10^{-2} µmol m^{-2}). This can be attributed to the slightly positive value of zeta potential (Figure S2, ESI), leading to repulsion, and lower adsorption on calcined samples. Even though the change in properties of TNT materials in case of calcination was mainly appointed to a partial change in crystal phase (formation of anatase), it is clear from the results that strongly altered surface properties have been generated compared to the not calcined materials but also in comparison to Anatase, which has a clearly negative zeta potential.

To conclude, for all tested nanomorphologies adsorption is higher in the water media with natural pH. Moreover, the tendency of Rh6G adsorption onto various solids is observed as follows: nanofibres ES >> nanopowder P25 > nanotubes TNT > nanopowder Anatase. This result can be related with structural properties of each solid. From Table 1, it can be noted that the nanotubes TNT have the highest specific surface areas, nevertheless, the amount adsorbed is not

the highest on this type of adsorbents. It is also interesting to observe that the percentage of rutile phase is increased in the materials with higher adsorption properties (i.e. ES and P25), while percentage of anatase phase is decreased in these two samples.

4. Conclusions

Titanium oxide nanoparticles with different morphologies have been employed for the removal of organic dye Rh6G. Nanotubes and ES nanofibres were synthesized by hydrothermal and electrospinning methods. Commercial nanopowder P25, as best photocatalytic material, was used as reference solid together with commercial Anatase. At first structural characterization of these adsorbed were performed before isothermal adsorption investigation.

Adsorption isotherms were carried out with batch-mode experiments from the water at natural pH and from phosphate buffer at pH 6 and pH 8. The results have shown that increasing the buffer pH from 6 to 8 give rise to the increase of adsorption capacity for P25 and ES nanofibres, due to the negative surface charge. That is in a good agreement with the results of zeta potential measurements. Nevertheless, this influence of pH is rather small, especially in the case of Anatase. Indeed, Anatase exhibits great adsorption capacity for phosphate. This thus clarifies the low affinity for Rh6G in the presence of PO_4^{3-}, because of the competition between anionic species. At pH 6 in water and in phosphate buffer, the adsorption capacity is also reduced, due to a combined effect of surface charge increase, in addition with the adsorption of competing ions. This could explain the modification of the catalytic performances. Adsorption from water at natural pH compared to adsorption in buffer has shown the presence of competitive adsorption between Rh6G and phosphates species on the surface of the TiO_2. The best adsorption capacity was achieved by ES nanofibres.

Supplementary Materials: The following are available online at Figure S1: Adsorption isotherms for Rhodamine 6G onto Anatase Commercial nanoparticles at 25°C from water at natural pH, from phosphate buffer at pH 6 and at pH 8, and Figure S2: Zeta-potential measurements in water with pH=8 (full symbols), and in phosphate buffer at pH=8 (empty symbols).

Acknowledgments: The research leading to these results has received funding from the European Research Council under the European Union's Seventh Framework Programme (FP/2007-2013) / ERC Grant Agreement n. 306682. Funds were received to cover the costs to publish in open access. Ganna Darmograi acknowledges a doctoral fellowship from the French government.

[1] A.L. Linsebigler, G.Q. Lu, J.T. Yates, Photocatalysis on TiO_2 surfaces - Principles, Mechanisms, and selected results, Chemical Reviews, 95 (1995) 735-758.
[2] P. Pattanaik, M.K. Sahoo, TiO_2 photocatalysis: progress from fundamentals to modification technology, Desalination and Water Treatment, 52 (2013) 6567-6590.
[3] A. Pal, T.K. Jana, K. Chatterjee, Silica supported TiO2 nanostructures for highly efficient photocatalytic application under visible light irradiation, Mater. Res. Bull., 76 (2016) 353-357.
[4] J. Schneider, M. Matsuoka, M. Takeuchi, J. Zhang, Y. Horiuchi, M. Anpo, D.W. Bahnemann, Understanding TiO_2 Photocatalysis: Mechanisms and Materials, Chemical Reviews, 114 (2014) 9919-9986.
[5] K. Bourikas, C. Kordulis, A. Lycourghiotis, Titanium Dioxide (Anatase and Rutile): Surface Chemistry, Liquid–Solid Interface Chemistry, and Scientific Synthesis of Supported Catalysts, Chemical Reviews, 114 (2014) 9754-9823.
[6] J. Sun, X. Yan, K. Lv, S. Sun, K. Deng, D. Du, Photocatalytic degradation pathway for azo dye in TiO_2/UV/O_3 system: Hydroxyl radical versus hole, Journal of Molecular Catalysis A: Chemical, 367 (2013) 31-37.
[7] H. Tada, M. Akazawa, Y. Kubo, S. Ito, Enhancing effect of SiOx monolayer coverage of TiO_2 on the photoinduced oxidation of rhodamine 6G in aqueous media, J. Phys. Chem. B, 102 (1998) 6360-6366.
[8] L.L. Bao, M.J. Meng, K.Y. Sun, W.B. Li, D.X. Zhao, H.M. Li, M.Q. He, Selective Adsorption and Degradation of Rhodamine B with Modified Titanium Dioxide Photocatalyst, J. Appl. Polym. Sci., 131 (2014) 12.
[9] K. Lv, J. Yu, K. Deng, J. Sun, Y. Zhao, D. Du, M. Li, Synergistic effects of hollow structure and surface fluorination on the photocatalytic activity of titania, J Hazard Mater, 173 (2010) 539-543.
[10] M.M. Khin, A.S. Nair, V.J. Babu, R. Murugan, S. Ramakrishna, A review on nanomaterials for environmental remediation, Energy Environ. Sci., 5 (2012) 8075-8109.
[11] X.D. Wang, Z.D. Li, J. Shi, Y.H. Yu, One-Dimensional Titanium Dioxide Nanomaterials: Nanowires, Nanorods, and Nanobelts, Chemical Reviews, 114 (2014) 9346-9384.
[12] S. Cavaliere, S. Subianto, I. Savych, D.J. Jones, J. Rozière, Electrospinning: designed architectures for energy conversion and storage devices, Energy Environ. Sci., 4 (2011) 4761-4785.
[13] S. Cavaliere, S. Subianto, L. Chevallier, D. Jones, J. Rozière, Single step elaboration of size-tuned Pt loaded titania nanofibres, Chem. Commun., 47 (2011) 6834-6836.
[14] A.K. Alves, F.A. Berutti, F.J. Clemens, T. Graule, C.P. Bergmann, Photocatalytic activity of titania fibers obtained by electrospinning, Mater. Res. Bull., 44 (2009) 312-317.
[15] Q. Li, D. Sun, H. Kim, Fabrication of porous TiO2 nanofiber and its photocatalytic activity, Mater. Res. Bull., 46 (2011) 2094-2099.
[16] V. Bem, M.C. Neves, M.R. Nunes, A.J. Silvestre, O.C. Monteiro, Influence of the sodium/proton replacement on the structural, morphological and photocatalytic properties of titanate nanotubes, Journal of Photochemistry and Photobiology A: Chemistry, 232 (2012) 50-56.
[17] W. Chang, F. Xu, X. Mu, L. Ji, G. Ma, J. Nie, Fabrication of nanostructured hollow TiO2 nanofibers with enhanced photocatalytic activity by coaxial electrospinning, Mater. Res. Bull., 48 (2013) 2661-2668.

[18] Q. Yuan, N. Li, W. Geng, Y. Chi, X. Li, Preparation of magnetically recoverable Fe_3O_4@SiO_2@meso-TiO_2 nanocomposites with enhanced photocatalytic ability, Mater. Res. Bull., 47 (2012) 2396-2402.
[19] C. Liu, X. Lin, Y. Li, P. Xu, M. Li, F. Chen, Enhanced photocatalytic performance of mesoporous TiO_2 coated SBA-15 nanocomposites fabricated through a novel approach: supercritical deposition aided by liquid-crystal template, Mater. Res. Bull., 75 (2016) 25-34.
[20] Y. Li, N. Li, J. Tu, X. Li, B. Wang, Y. Chi, D. Liu, D. Yang, TiO_2 supported on rod-like mesoporous silica SBA-15: Preparation, characterization and photocatalytic behaviour, Mater. Res. Bull., 46 (2011) 2317-2322.
[21] T. Balaganapathi, B. KaniAmuthan, S. Vinoth, P. Thilakan, Synthesis, characterization and dye adsorption studies of porous brookite and mixed brookite with rutile TiO2 using PEG assisted sol-gel synthesis process, Mater. Res. Bull., 91 (2017) 114-121.
[22] M. Ali Ahmad, B. Prelot, A. Razafitianamaharavo, J.M. Douillard, J. Zajac, F. Dufour, O. Durupthy, C. Chanéac, F. Villiéras, Influence of Morphology and Crystallinity on Surface Reactivity of Nanosized Anatase TiO_2 Studied by Adsorption Techniques. 1. The Use of Gaseous Molecular Probes. , The Journal of Physical Chemistry C, 116 (2012) 24596−24606.
[23] N.B. Shali, S. Sugunan, Influence of transition metals on the surface acidic properties of titania prepared by sol–gel route, Mater. Res. Bull., 42 (2007) 1777-1783.
[24] M. Ali Ahmad, B. Prelot, F. Dufour, O. Durupthy, A. Razafitianamaharavo, J.M. Douillard, C. Chaneac, F. Villiéras, J. Zajac, Influence of Morphology and Crystallinity on Surface Reactivity of Nanosized Anatase TiO_2 Studied by Adsorption Techniques. 2. Solid–Liquid Interface, The Journal of Physical Chemistry C, 117 (2013) 4459-4469.
[25] X. Zhang, J. Yao, D. Li, X. Chen, H. Wang, L.Y. Yeo, J.R. Friend, Self-assembled highly crystalline TiO_2 mesostructures for sunlight-driven, pH-responsive photodegradation of dyes, Mater. Res. Bull., 55 (2014) 13-18.
[26] L. Chang, F. Wang, D. Xie, J. Zhang, G. Du, Graphite oxide-mediated synthesis of porous CeO_2 quadrangular prisms and their high-efficiency adsorptive performance, Mater. Res. Bull., 48 (2013) 4362-4367.
[27] G. Liu, H.G. Yang, J. Pan, Y.Q. Yang, G.Q. Lu, H.-M. Cheng, Titanium Dioxide Crystals with Tailored Facets, Chemical Reviews, 114 (2014) 9559-9612.
[28] J. Cunningham, G. Al-Sayyed, Factors influencing efficiencies of TiO_2-sensitized photodegradation. Part 1.-Substituted benzoic acids: discrepancies with dark-adsorption parameters, Journal of the Chemical Society, Faraday Transactions, 86 (1990) 3935-3941.
[29] J.-K. Yang, A.P. Davis, Competitive Adsorption of Cu(II)–EDTA and Cd(II)–EDTA onto TiO2, Journal of Colloid and Interface Science, 216 (1999) 77-85.
[30] N. Lee, D.A. Sverjensky, R.M. Hazen, Cooperative and Competitive Adsorption of Amino Acids with Ca^{2+} on Rutile (α-TiO_2), Environmental Science & Technology, 48 (2014) 9358-9365.
[31] L. Weng, W.H. Van Riemsdijk, T. Hiemstra, Humic nanoparticles at the oxide−water interface: Interactions with phosphate ion adsorption, Environmental Science & Technology, 42 (2008) 8747-8752.
[32] M. Erhayem, M. Sohn, Effect of humic acid source on humic acid adsorption onto titanium dioxide nanoparticles, Science of The Total Environment, 470–471 (2014) 92-98.
[33] M. Fehse, S. Cavaliere, P.E. Lippens, I. Savych, A. Iadecola, L. Monconduit, D.J. Jones, J. Rozière, F. Fischer, C. Tessier, L. Stievano, Nb-Doped TiO_2 Nanofibers for Lithium Ion Batteries, The Journal of Physical Chemistry C, 117 (2013) 13827-13835.

[34] S. Ribbens, V. Meynen, G.V. Tendeloo, X. Ke, M. Mertens, B.U.W. Maes, P. Cool, E.F. Vansant, Development of photocatalytic efficient Ti-based nanotubes and nanoribbons by conventional and microwave assisted synthesis strategies, Microporous and Mesoporous Materials, 114 (2008) 401-409.
[35] S. Ribbens, I. Caretti, E. Beyers, S. Zamani, E. Vinck, S. Van Doorslaer, P. Cool, Unraveling the Photocatalytic Activity of Multiwalled Hydrogen Trititanate and Mixed-Phase Anatase/Trititanate Nanotubes: A Combined Catalytic and EPR Study, The Journal of Physical Chemistry C, 115 (2011) 2302-2313.
[36] I. Savych, J. Bernard d'Arbigny, S. Subianto, S. Cavaliere, D.J. Jones, J. Rozière, On the effect of non-carbon nanostructured supports on the stability of Pt nanoparticles during voltage cycling: A study of TiO_2 nanofibres, Journal of Power Sources, 257 (2014) 147-155.
[37] K. Mogyorosi, N. Balazs, D.F. Sranko, E. Tombacz, I. Dekany, A. Oszko, P. Sipos, A. Dombi, The effect of particle shape on the activity of nanocrystalline TiO_2 photocatalysts in phenol decomposition. Part 3: The importance of surface quality, Appl. Catal. B-Environ., 96 (2010) 577-585.
[38] S. Hamad, J.R. Sanchez-Valencia, A. Barranco, J.A. Mejias, A.R. Gonzalez-Elipe, Molecular dynamics simulation of the effect of pH on the adsorption of rhodamine laser dyes on TiO_2 hydroxylated surfaces, Mol. Simul., 35 (2009) 1140-1151.
[39] P. Connor, A.J. McQuillan, Phosphate adsorption onto TiO_2 from aqueous solutions: an in situ internal reflection infrared spectroscopic study, Langmuir, 15 (1999) 2916-2921.

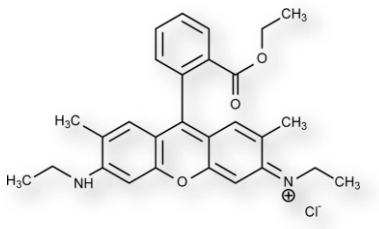

Figure 1. Molecular structure of Rhodamine 6G

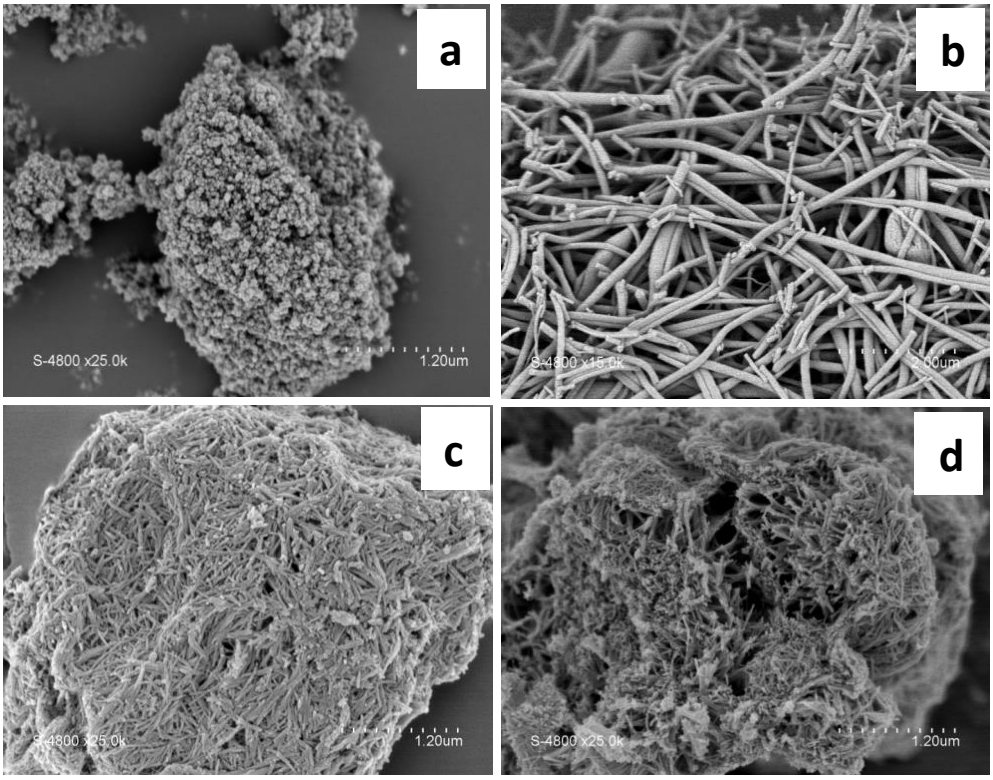

Figure 2. SEM images of Anatase (a), ES nanofibres (b) and nanotubes calcined (c) and not calcined (d).

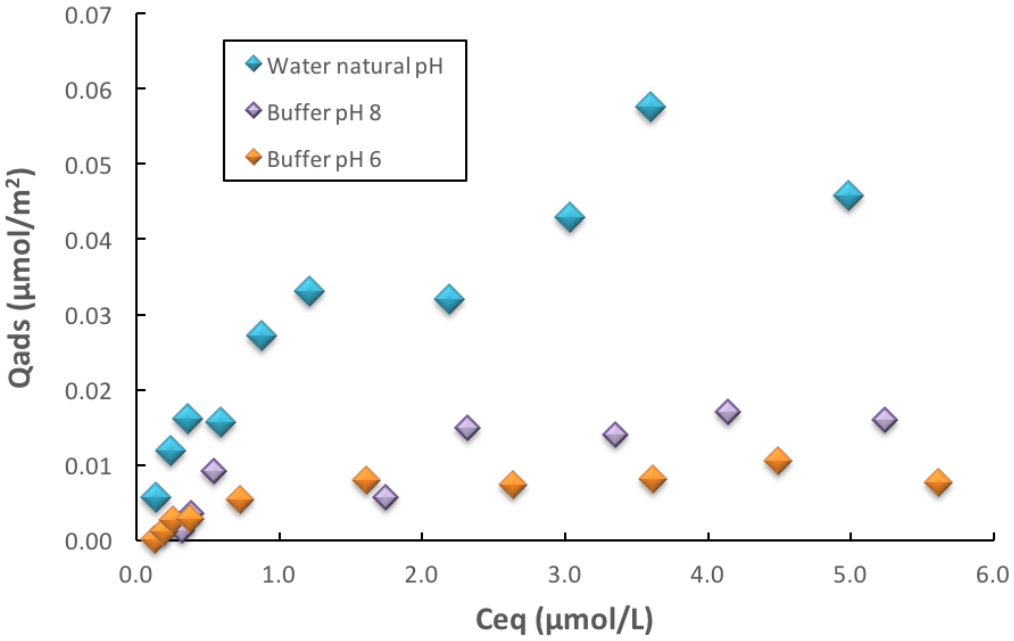

Figure 3. Adsorption isotherms for Rhodamine 6G onto P25 nanoparticles at 25°C from water at natural pH, from phosphate buffer at pH 6 and at pH 8.

A **B**

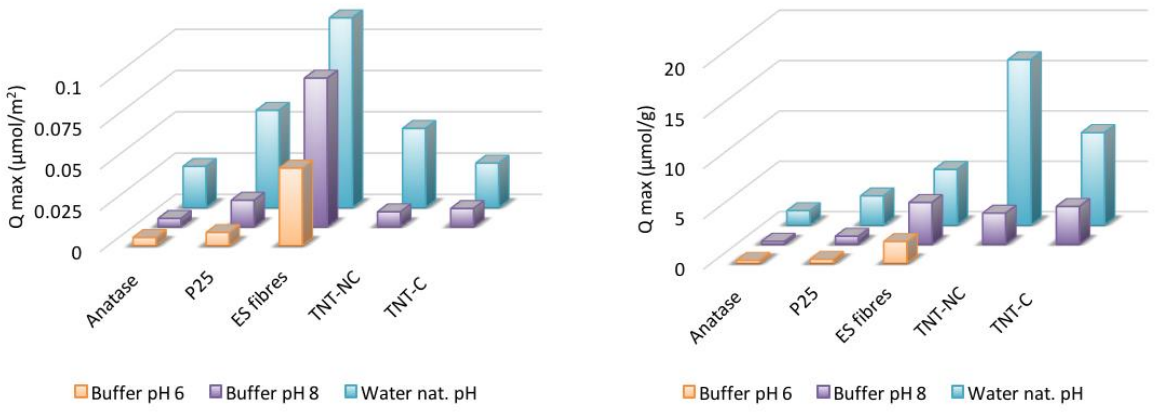

Figure 4. Maximum amounts of dye adsorbed onto titanate and titanium oxide samples from water at natural pH and from phosphate buffer solutions at pH 8 and pH 6, expressed in µmol per square meter (A) or µmol per gram (B).

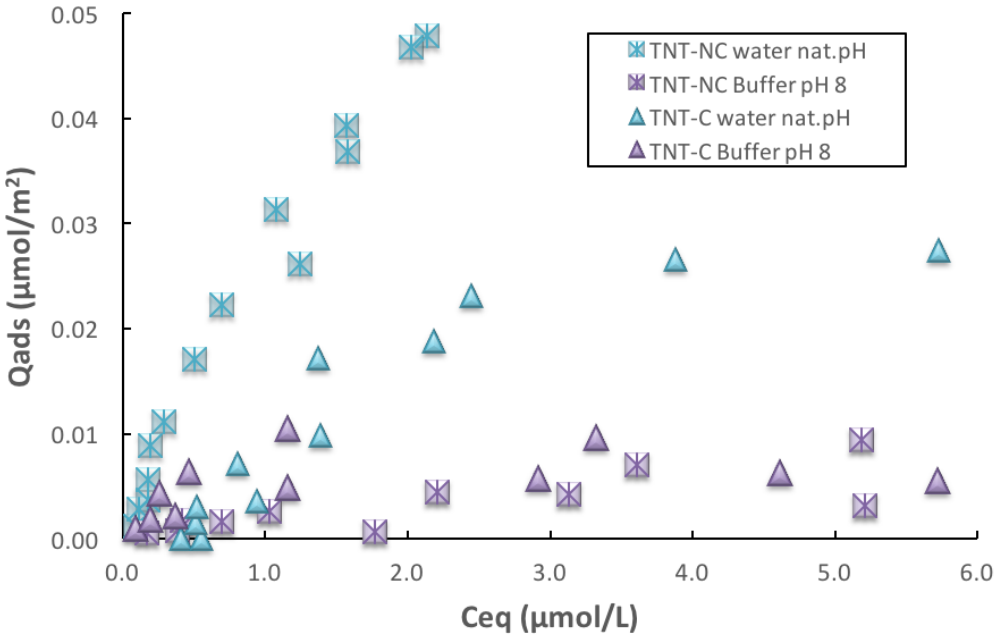

Figure 5. Adsorption isotherms for Rhodamine 6G onto nanotubes TNT-NC and TNT-C at 25°C from water at natural pH and from phosphate buffer at pH8.

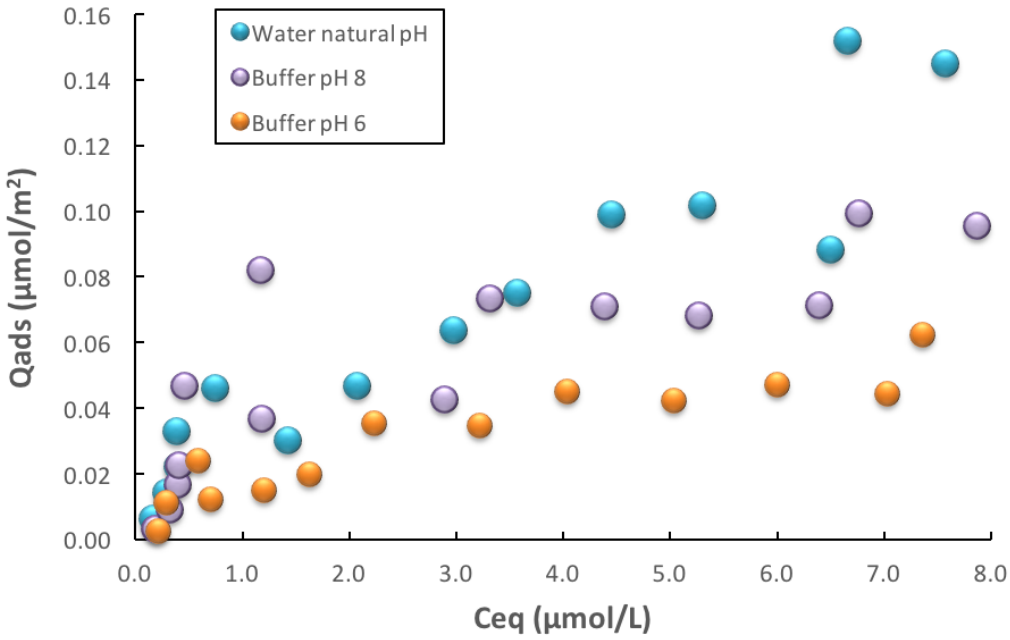

Figure 6. Adsorption isotherms for Rhodamine 6G onto ES Nanofibres at 298 K from water at natural pH, from phosphate buffer at pH 6 and at pH 8.

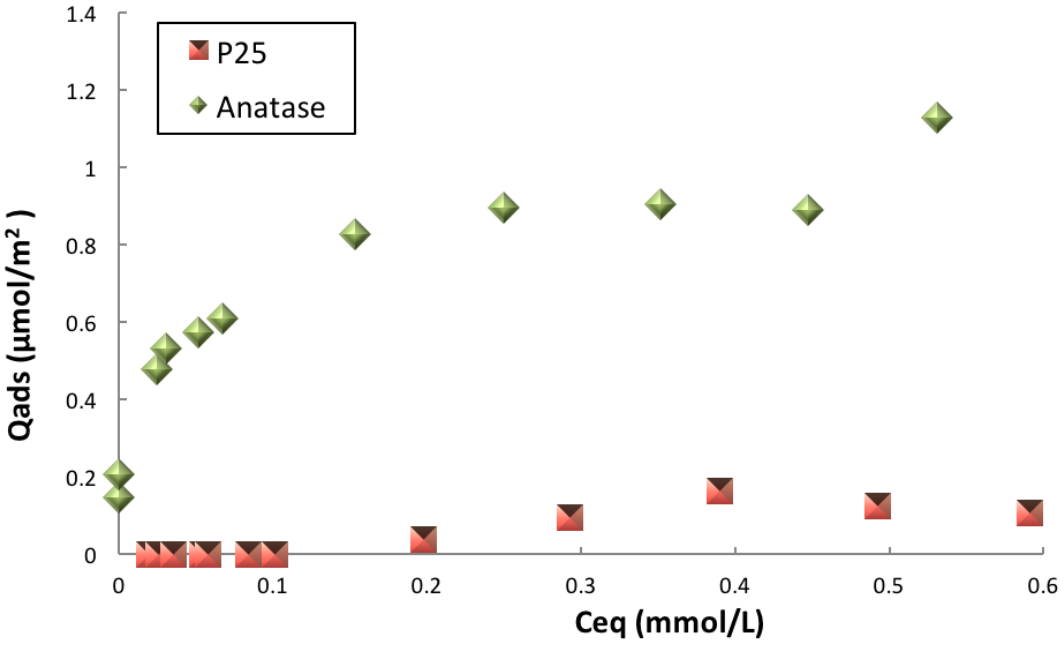

Figure 7. Adsorption isotherms for HPO_4^{2-} onto P25 and Commercial Anatase nanoparticles at 25°C from water at natural pH.

Table 1. Specific surface area and crystal phase of the various titanium oxide samples.

Sample name	Crystal phase [a]	S_{BET} ($m^2 g^{-1}$)
Anatase Commercial	100% anatase	57
P25	81% anatase 19% rutile	49
ES nanofibres	68% anatase 32% rutile	46
TNT-NC	TNT	342
TNT-C	TNT + Anatase	340

[a] Crystal phase determined with XRD or FT-Raman Spectroscopy [35]